

An exactly solvable \mathcal{PT} -symmetric dimer from a Hamiltonian system of nonlinear oscillators with gain and loss

I V Barashenkov

*Department of Mathematics and Centre for Theoretical and Mathematical Physics,
University of Cape Town, Rondebosch 7701, South Africa*

Mariagiovanna Gianfreda

Department of Physics, Washington University, St. Louis, MO 63130, USA

We show that a pair of coupled nonlinear oscillators, of which one oscillator has positive and the other one negative damping of equal rate, can form a Hamiltonian system. Small-amplitude oscillations in this system are governed by a \mathcal{PT} -symmetric nonlinear Schrödinger dimer with linear and cubic coupling. The dimer also represents a Hamiltonian system and is found to be exactly solvable in elementary functions. We show that the nonlinearity softens the \mathcal{PT} -symmetry breaking transition in the nonlinearly-coupled dimer: stable periodic and quasiperiodic states with large enough amplitudes persist for an arbitrarily large value of the gain-loss coefficient.

I. INTRODUCTION

Originally introduced as a concept in quantum mechanics [1], the idea of \mathcal{PT} symmetry has expanded into a wide range of fundamental and applied sciences, most notably photonics [2–4], plasmonics [5], quantum optics of atomic gases [6], studies of the Bose-Einstein condensation [7, 8], and physics of electronic circuits [9]. The \mathcal{PT} -symmetric equations model physical structures with balanced gain and loss. These lie halfway between open systems (systems in contact with external environment) and closed, isolated, settings. Increasing the gain-loss rate takes the structure from the unbroken \mathcal{PT} -symmetry phase, characterised by stationary, periodic or quasiperiodic evolution, to the symmetry-broken phase, where it is in the uncontrollable blow-up regime.

The transition between the two phases has been observed in a variety of experimental environments including optics [2, 3], superconductivity [10], microwave cavities [11], atomic diffusion [12], and nuclear magnetic resonance [13]. In particular, the \mathcal{PT} -symmetric phase transition is easily recognised in structures consisting of coupled oscillators with gain and loss [9, 14–16]. A theoretical modelling of this experimental setting [15] has demonstrated that two coupled linear oscillators with balanced gain and loss can form a Hamiltonian system [17].

The system considered in [17] (see also [9]) had the form

$$\begin{aligned}\ddot{x} + 2\eta\dot{x} + x + 2\kappa y &= 0, \\ \ddot{y} - 2\eta\dot{y} + y + 2\kappa x &= 0.\end{aligned}\quad (1)$$

Here x and y are the coordinates of two coupled harmonic oscillators — or the two degrees of freedom of a particle in a parabolic well. The coefficient $\eta > 0$ gives the rate of damping experienced by the x -component and, at the same time, quantifies the energy gain by the component y . The coefficient $\kappa > 0$ measures the coupling between the two components. Finally, the overdot stands for the derivative in t .

Given the fact that there are channels both for the gain and loss of energy, the availability of the Hamiltonian for (1) is surprising and counter-intuitive. A natural question, therefore, is how structurally stable this property is. Will the Hamiltonian structure survive the addition of nonlinear terms? If yes, how different are dynamical and bifurcation properties of the Hamiltonian \mathcal{PT} -symmetric system from those of its non-Hamiltonian counterparts?

The first of these two questions is answered here by devising a Hamiltonian system of two coupled cubic oscillators whose linear truncation is given by Eq.(1). Assuming that the gain-loss coefficient is small while the coupling is weak, we show that the amplitude of the small-amplitude oscillations in this system satisfies a two-site discrete nonlinear Schrödinger equation with gain in one site and loss in the other. Like the parent system of two coupled oscillators, this \mathcal{PT} -symmetric Schrödinger dimer is Hamiltonian; furthermore, the dimer is found to be exactly solvable in elementary functions. The bulk of our paper is concerned with the analysis of this new discrete nonlinear Schrödinger equation.

We compare the Hamiltonian \mathcal{PT} -symmetric dimer — which features a *nonlinear* coupling of the two sites in addition to the standard, linear, coupling — to the previously considered *linearly*-coupled \mathcal{PT} -symmetric Schrödinger model. One of the striking differences between the two systems is that all stationary states in the new dimer are stable. The other one is that the nonlinearity softens the \mathcal{PT} -symmetric phase transition in the new model. By this, we mean that the increase of the gain-loss coefficient beyond the point of the linear \mathcal{PT} -phase transition does not eliminate stable stationary and periodic states with large amplitudes. Stable bounded solutions persist for an arbitrarily large value of the gain-loss coefficient.

The outline of this paper is as follows. In section II we introduce our Hamiltonian system of two coupled anharmonic oscillators with positive and negative damping. Subsequently (section III) the two-oscillator system is reduced to a \mathcal{PT} -symmetric discrete Schrödinger equa-

tion for the amplitudes of small x - and y -oscillations. In section IV we obtain, explicitly, the general solution of this Schrödinger dimer and in section V classify its most important, stationary, regimes. (Technical details of the fixed-point analysis have been relegated to two appendices.) The bifurcation diagram for the stationary regimes is compared to the corresponding diagram for the linearly-coupled dimer (section VI). Finally, section VII summarises results of this project.

II. HAMILTONIAN SYSTEM OF TWO OSCILLATORS WITH GAIN AND LOSS

The system we propose as a nonlinear extension of Eqs.(1), is

$$\begin{aligned} \ddot{x} + 2\eta\dot{x} + x + 2\kappa y + x(x^2 + 3y^2) &= 0, \\ \ddot{y} - 2\eta\dot{y} + y + 2\kappa x + y(y^2 + 3x^2) &= 0. \end{aligned} \quad (2)$$

The system (2) is \mathcal{PT} -symmetric, that is, invariant under the joint action of the \mathcal{P} and \mathcal{T} transformations. Here \mathcal{P} is the operator that swaps the x and y components, and \mathcal{T} is the time inversion: $\mathcal{T}x(t) = x(-t)$, $\mathcal{T}y(t) = y(-t)$.

One can readily check that the cubic system (2) is also Hamiltonian, with the Hamilton function

$$H = pq - \eta(xp - yq) + (1 - \eta^2)xy + \kappa(x^2 + y^2) + xy^3 + x^3y.$$

One pair of the Hamilton equations is

$$\dot{x} = \frac{\partial H}{\partial p} = q - \eta x, \quad \dot{y} = \frac{\partial H}{\partial q} = p + \eta y.$$

These express the canonical momenta in terms of the velocities:

$$q = \dot{x} + \eta x, \quad p = \dot{y} - \eta y. \quad (3)$$

The second pair is

$$\dot{p} = -\frac{\partial H}{\partial x}, \quad \dot{q} = -\frac{\partial H}{\partial y}. \quad (4)$$

Substituting (3) in (4) gives the system (2).

There is an extensive literature on *quantum* \mathcal{PT} -symmetric Hamiltonians (see e.g. [18]). In particular, a well established fact is that a \mathcal{PT} -symmetric Hamiltonian operator can be related to an equivalent isospectral Hermitian Hamiltonian by a similarity transformation [19]. At the *classical* level, the studies of \mathcal{PT} -symmetric Hamiltonian systems were confined to formal aspects such as trajectories on the complex plane [20]. So far, the only example of a real classical \mathcal{PT} -symmetric system with loss and gain that admits a Hamiltonian formulation, was the set of linear equations (1). Equations (2) constitute the first example of a nonlinear system of that kind.

III. \mathcal{PT} -SYMMETRIC DIMER

Linearising Eqs.(2) about the trivial fixed point $x = y = 0$, the stability eigenvalues are found to be

$$(\lambda^2)_{1,2} = 2\eta^2 - 1 \pm 2\sqrt{\kappa^2 - \eta^2(1 - \eta^2)}.$$

The fixed point is stable if both values for λ^2 are real and nonpositive; this happens if the following two conditions are met simultaneously:

$$\eta^2 \leq \frac{1}{2}, \quad \eta^2(1 - \eta^2) \leq \kappa^2 \leq \frac{1}{4}. \quad (5)$$

In this study, we restrict ourselves to small η and κ . According to Eq.(5), there is a subregion of the small-parameter domain where the fixed point is stable (a centre). With η and κ chosen in the stability subregion, we expect to find bounded motions in a neighbourhood of the fixed point. To construct these quasiperiodic orbits, and examine their stability, we use the multiple scale expansion.

Letting

$$2\kappa = K\epsilon^2, \quad 2\eta = \Gamma\epsilon^2, \quad (6)$$

we expand x and y in odd powers of ϵ :

$$x = \epsilon x_1 + \epsilon^3 x_3 + \dots, \quad y = \epsilon y_1 + \epsilon^3 y_3 + \dots \quad (7)$$

Assuming that x_i and y_i depend on a hierarchy of time scales, $T_0 = t$, $T_{2n} = \epsilon^{2n}t$ ($n = 1, 2, \dots$), gives

$$\frac{d}{dt} = D_0 + \epsilon^2 D_2 + \dots; \quad \frac{d^2}{dt^2} = D_0^2 + 2\epsilon^2 D_0 D_2 + \dots \quad (8)$$

Substituting (6)-(8) in (2), we equate coefficients of like powers of ϵ .

The order ϵ^1 produces

$$(D_0^2 + 1)x_1 = (D_0^2 + 1)y_1 = 0,$$

whence

$$x_1 = \mathcal{A}e^{iT_0} + c.c., \quad y_1 = \mathcal{B}e^{iT_0} + c.c.. \quad (9)$$

Here $\mathcal{A} = \mathcal{A}(T_2, T_4, \dots)$, $\mathcal{B} = \mathcal{B}(T_2, T_4, \dots)$, and *c.c.* stands for the complex conjugate of the preceding term. At the order ϵ^3 we obtain

$$\begin{aligned} (D_0^2 + 1)x_3 + (2D_0D_2 + \Gamma D_0)x_1 + Ky_1 + x_1^3 + 3y_1^2x_1 &= 0, \\ (D_0^2 + 1)y_3 + (2D_0D_2 - \Gamma D_0)y_1 + Kx_1 + y_1^3 + 3x_1^2y_1 &= 0. \end{aligned}$$

Substituting for x_1 and y_1 from (9), and setting the secular terms to zero results in

$$\begin{aligned} 2iD_2\mathcal{A} + i\Gamma\mathcal{A} + K\mathcal{B} + 3(|\mathcal{A}|^2 + 2|\mathcal{B}|^2)\mathcal{A} + 3\mathcal{B}^2\mathcal{A}^* &= 0, \\ 2iD_2\mathcal{B} - i\Gamma\mathcal{B} + K\mathcal{A} + 3(2|\mathcal{A}|^2 + |\mathcal{B}|^2)\mathcal{B} + 3\mathcal{A}^2\mathcal{B}^* &= 0. \end{aligned}$$

Letting $\tau = KT_2/2$, defining $\gamma = \Gamma/K$, and scaling the amplitude components as $\mathcal{A} = (K/3)^{1/2}\psi_1$ and $\mathcal{B} = (K/3)^{1/2}\psi_2$, these equations acquire the form

$$\begin{aligned} i\dot{\psi}_1 + \psi_2 + (|\psi_1|^2 + 2|\psi_2|^2)\psi_1 + \psi_2^2\psi_1^* &= -i\gamma\psi_1, \\ i\dot{\psi}_2 + \psi_1 + (|\psi_2|^2 + 2|\psi_1|^2)\psi_2 + \psi_1^2\psi_2^* &= i\gamma\psi_2. \end{aligned} \quad (10)$$

(Here and below the overdot is used to denote the derivative with respect to τ .)

The system (10) is in the form of a two-site discrete nonlinear Schrödinger equation, the so-called nonlinear Schrödinger dimer. Dimers with various nonlinearities are workhorses of photonics, where they serve to model stationary light beams in coupled optical waveguides [3, 21–23]. (Similar equations govern electromagnetic waves with orthogonal polarisations propagating in a single-mode nonlinear fiber, see e.g. [24].) The coupler described by (10) consists of a waveguide with loss and a guide with an equal amount of optical gain. The variables ψ_1 and ψ_2 represent the corresponding complex beam amplitudes, $\gamma > 0$ is their common gain-loss rate, and τ measures the distance along the parallel cores. The quantities $P_2 = |\psi_2|^2$ and $P_1 = |\psi_1|^2$ give the powers carried by the active and lossy channel, respectively.

Another area where the nonlinear Schrödinger dimers occur commonly, comprises the studies of the boson condensation [8, 25]. In particular, the nonlinearity (10) describes the mean-field condensate wave function in a symmetric double-well potential in the two-mode approximation [26]. The ψ_1 and ψ_2 are the complex amplitudes of the ground and the first excited state, respectively. In the matter-wave context, P_1 and P_2 are the numbers of particles associated with the two modes.

The dynamical regimes in Eqs.(10) are selected by varying the gain-loss rate, γ . This is a single parameter in the system. We note that γ admits a simple expression in terms of the parameters of the original two-oscillator model (2): $\gamma = \eta/\kappa$.

As its parent system (2), the dimer (10) is \mathcal{PT} -symmetric. Here the \mathcal{P} operator is defined by

$$\mathcal{P} \begin{pmatrix} \psi_1 \\ \psi_2 \end{pmatrix} = \begin{pmatrix} \psi_2 \\ \psi_1 \end{pmatrix}. \quad (11)$$

If ψ_1 and ψ_2 are interpreted as the mode amplitudes in two parallel waveguides, this operator performs the spatial reflection in the direction perpendicular to the cores. On the other hand, the \mathcal{T} operator represents the effect of the time inversion on the complex amplitudes: $\mathcal{T}\psi_n(\tau) = \psi_n^*(-\tau)$, $n = 1, 2$.

Like the original equations (2) for two anharmonic oscillators, their amplitude system (10) is Hamiltonian. It can be written as

$$i\dot{\psi}_1 = -\frac{\partial\mathcal{H}}{\partial\psi_2^*}, \quad i\dot{\psi}_2 = -\frac{\partial\mathcal{H}}{\partial\psi_1^*},$$

where the Hamilton function

$$\begin{aligned} \mathcal{H} = (|\psi_1|^2 + |\psi_2|^2)(1 + \psi_1^*\psi_2 + \psi_1\psi_2^*) \\ + i\gamma(\psi_1\psi_2^* - \psi_1^*\psi_2). \end{aligned} \quad (12)$$

IV. EXACT LINEARISATION OF THE DIMER

The trivial fixed point of the dynamical system (10) is $\psi_1 = \psi_2 = 0$. In the region $\gamma > 1$, the fixed point is unstable (a saddle). With reference to small initial conditions, for which the nonlinear terms are negligible, it is common to say that the \mathcal{PT} -symmetry is spontaneously broken here. The term means to indicate that generic small perturbations experience exponential growth. In the region $\gamma \leq 1$, the trivial fixed point is stable (a centre) and the symmetry is said to be unbroken. Small perturbations remain small as $\tau \rightarrow \infty$.

Large initial conditions in a nonlinear Schrödinger dimer may lead to an exponential blowup — similar to the blowup in the symmetry-broken linear dimer — but also may give rise to stable periodic, quasiperiodic or chaotic orbits [27–30]. As a result, the \mathcal{PT} -symmetry breaking transition may be softened by the nonlinearity. In order to understand details of the phase transition in systems modelled by the \mathcal{PT} -symmetric dimer (10), we obtain its complete solution here.

Introducing the Stokes variables

$$X = 2(|\psi_1|^2 - |\psi_2|^2), \quad Y = 2i(\psi_1^*\psi_2 - \psi_1\psi_2^*),$$

and

$$Z = 2(\psi_1^*\psi_2 + \psi_1\psi_2^*),$$

equations (10) can be written as a three-dimensional dynamical system:

$$\dot{X} = -2\gamma r + (2 + Z)Y, \quad (13a)$$

$$\dot{Y} = -(2 + Z)X, \quad (13b)$$

$$\dot{Z} = 0. \quad (13c)$$

Here r is the length of the vector $\vec{r} = (X, Y, Z)$:

$$r = \sqrt{X^2 + Y^2 + Z^2} = 2(|\psi_1|^2 + |\psi_2|^2). \quad (14)$$

The length satisfies

$$\dot{r} = -2\gamma X. \quad (15)$$

Eq.(13c) implies that Z is a conserved quantity, and so all trajectories lie on the horizontal planes $Z = \text{const}$. Another conserved quantity is

$$\mathcal{H} = \frac{r}{2} \left(1 + \frac{Z}{2} \right) - \frac{\gamma}{2} Y;$$

this is nothing but the Hamilton function (12). The existence of two integrals of motion establishes the complete integrability of the system (13) and the dimer (10).

We can treat r as an independent variable and add the evolution equation (15) to the system (13). The four-dimensional system (13),(15) has one more integral of motion, $I = X^2 + Y^2 + Z^2 - r^2$; solutions of the three-dimensional system (13) are selected by considering the

invariant manifold $I = 0$ and restricting to $r \geq 0$. The advantage of the four-dimensional formulation is that it reveals the hidden linearity of the system (13).

Eliminating Y and r from (13a), (13b) and (15), we obtain an equation of harmonic oscillator or inverted oscillator,

$$\ddot{X} + \nu^2 X = 0,$$

depending on whether

$$\nu^2 = (2 + Z)^2 - 4\gamma^2$$

is positive or negative. Once the two-parameter family of solutions for $X(\tau)$ has been written down, Eqs.(13b) and (15) can be used to recover the corresponding $Y(\tau)$.

Assume, first, that $(2 + Z)^2 > 4\gamma^2$, that is, consider Z lying below $-2(\gamma + 1)$ or above $2(\gamma - 1)$. The general solution of the system (13) in this case is

$$\begin{aligned} X &= \rho_0 \cos \phi, \\ Y &= Y_0 - \frac{2 + Z}{\nu} \rho_0 \sin \phi, \end{aligned} \quad (16)$$

where $\phi = \nu(\tau - \tau_0)$,

$$Y_0 = \begin{cases} \frac{2\gamma}{\nu} \sqrt{\rho_0^2 + Z^2}, & Z > 2(\gamma - 1); \\ -\frac{2\gamma}{\nu} \sqrt{\rho_0^2 + Z^2}, & Z < -2(\gamma + 1), \end{cases} \quad (17)$$

and $\rho_0 > 0$, τ_0 are arbitrary constants of integration. Thus, each horizontal plane with $Z > 2(\gamma - 1)$ or $Z < -2(\gamma + 1)$ hosts a family of nested ellipses

$$X^2 + \left(\frac{\nu}{2 + Z} \right)^2 (Y - Y_0)^2 = \rho_0^2. \quad (18)$$

(See Fig.1.) The length of the \vec{r} -vector remains finite as the imaginary particle moves around the ellipse:

$$r(\tau) = \frac{2 + Z}{2\gamma} Y_0 - \frac{2\gamma}{\nu} \rho_0 \sin \phi.$$

In contrast, all motions corresponding to Z between $-2(\gamma + 1)$ and $2(\gamma - 1)$, are unbounded:

$$\begin{aligned} X &= -A \sinh s, \\ Y &= \frac{2 + Z}{\sigma} A \cosh s + Y_0, \end{aligned}$$

where $s = \sigma(\tau - \tau_0)$,

$$\begin{aligned} \sigma &= \sqrt{4\gamma^2 - (2 + Z)^2} > 0, \\ A &= \sqrt{Z^2 + \frac{\sigma^2}{4\gamma^2} Y_0^2} > 0, \end{aligned}$$

Y_0 can be chosen arbitrarily (positive or negative), and τ_0 is also an arbitrary parameter. The length of the vector \vec{r} in this case is given by

$$r = \frac{2\gamma}{\sigma} A \cosh s + \frac{2 + Z}{2\gamma} Y_0.$$

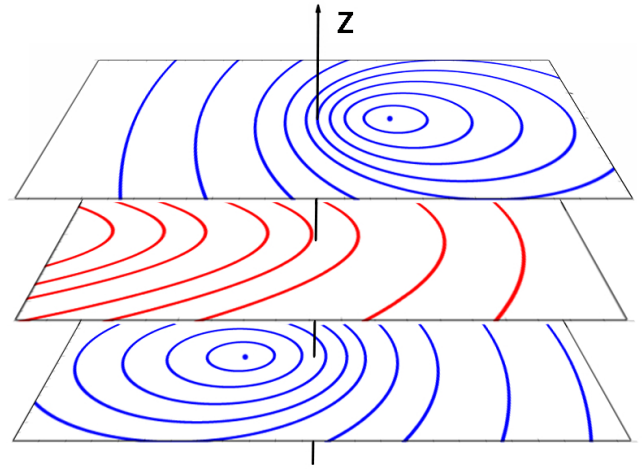


FIG. 1. The phase space of the system (13). All trajectories lie in the horizontal planes $Z = \text{const}$. The planes with $|Z + 2| > 2\gamma$ harbour only periodic orbits (solid/blue curves). In contrast, all motions found in the gap $|Z + 2| \leq 2\gamma$ are unbounded (dashed/red curves).

The solution blows up: $r \rightarrow \infty$ as $\tau \rightarrow \pm\infty$. (Fig.1.)

Once we have an explicit expression for the trajectory $\vec{r}(\tau)$, the corresponding dimer components $\psi_1 = \sqrt{P_1} e^{i\theta}$ and $\psi_2 = \sqrt{P_2} e^{i(\theta - \theta_0)}$ can be easily reconstructed:

$$\begin{aligned} P_1 &= \frac{r + X}{4}, \quad P_2 = \frac{r - X}{4}, \\ \cos \theta_0 &= \frac{Z}{\sqrt{Y^2 + Z^2}} \quad \sin \theta_0 = \frac{Y}{\sqrt{Y^2 + Z^2}}, \end{aligned}$$

and

$$\theta = \frac{1}{2} \int \left(r + Z \frac{Z + 2}{r + X} \right) d\tau. \quad (19)$$

Finally, we note that the above solution of the three-dimensional system is in agreement with the classification of the $\psi_{1,2} = 0$ fixed point in the beginning of this section. If $\gamma < 1$, the $(Z = 0)$ -plane lies above the $2(\gamma - 1)$ level. Hence the origin $X = Y = Z = 0$ is a centre in the $Z = 0$ plane; all trajectories on this and nearby horizontal planes are ellipses. In contrast, when $\gamma > 1$, the $(Z = 0)$ -plane lies below $2(\gamma - 1)$ but above the $-2(\gamma + 1)$ mark. In this case, the origin is a saddle in its “plane of residence”. Small initial conditions blow up: $r \rightarrow \infty$ as $\tau \rightarrow \infty$.

V. STATIONARY REGIMES OF THE DIMER

In addition to the trivial fixed point at the origin, the system (13) has a family of nontrivial fixed points (X_*, Y_*, Z) . There is one nontrivial fixed point lying on each horizontal plane $Z = \text{const}$ with Z satisfying

$$(2 + Z)^2 \geq 4\gamma^2.$$

The horizontal coordinates of the fixed point result by setting $\rho_0 = 0$ in (16) and (17):

$$X_* = 0, \quad Y_* = \begin{cases} \frac{2\gamma}{\nu}|Z|, & Z > 2(\gamma - 1); \\ -\frac{2\gamma}{\nu}|Z|, & Z < -2(\gamma + 1). \end{cases}$$

One readily verifies that for any ρ_0 , the distance of the fixed point to the centre of the corresponding ellipse is shorter than its Y -semiaxis:

$$|Y_* - Y_0| < \frac{|2 + Z|}{\nu} \rho_0.$$

That is, the fixed point is enclosed by the entire family of nested ellipses (18), see Fig.1. This means that the non-trivial fixed point is always stable (a nonlinear centre).

The fixed point of the three-dimensional system (13) corresponds to a periodic solution of the dimer (10). However, since the absolute values of the complex amplitudes $\psi_1 = \sqrt{P_1}e^{i\omega\tau}$ and $\psi_2 = \sqrt{P_2}e^{i(\omega\tau - \theta_0)}$ are time-independent, this periodic solution represents a stationary configuration of the condensate and describes a uniform, nonoscillatory, beam propagation in the optical coupler. For this reason we will be referring to this solution as the *stationary regime* of the dimer. Despite this physically appealing terminology, one should remember that mathematically, the stationary regime is a periodic solution with the associated frequency $\omega = \dot{\theta}$.

Note that equation $X_* = 0$ implies $P_1 = P_2$, that is, the two waveguides carry equal powers in the stationary regime. (Equivalently, the two modes of the condensate capture equal numbers of particles.)

As for the elliptic orbits of the three-dimensional system (13), these give rise to quasiperiodic solutions of the dimer. The corresponding $P_1(\tau)$ and $P_2(\tau)$ are periodic.

Fig.2(b) summarises these conclusions on the (γ, ω) plane. The plane has been divided into four domains, according to the number of coexisting stationary regimes with the same frequency ω . (The degenerate situation along the line $\gamma = 1$ has not been indicated.) The domain boundaries are bifurcation curves of the stationary solutions.

To classify the bifurcations, we note that eigenvalues of the linearisation matrix of Eq.(10),

$$\mathcal{L} = \begin{pmatrix} i\gamma & 1 \\ 1 & -i\gamma \end{pmatrix}, \quad (21)$$

are given by $\omega = \pm\sqrt{1 - \gamma^2}$. Assume $\gamma < 1$ is fixed and ω is increased. As ω passes through $-\sqrt{1 - \gamma^2}$ [the bottom boundary of the dark-grey region in Fig.2(b)], one stationary solution bifurcates from the eigenvector

$$\begin{pmatrix} \psi_1 \\ \psi_2 \end{pmatrix} = \begin{pmatrix} i\gamma - \sqrt{1 - \gamma^2} \\ 1 \end{pmatrix} \quad (22)$$

Physically, these represent longitudinal variations of the optical beam powers and periodic oscillations of the numbers of particles in the condensate.

The frequency $\omega = \dot{\theta}$ is a physically meaningful characteristic of the stationary regime — the propagation constant of the optical beam and the chemical potential in the condensate. Eq.(19) gives $\omega = \Omega(Z)$, where the function $\Omega(Z)$ is defined by

$$\Omega(Z) = \text{sign}[Z(Z + 2)] \frac{(Z + 2)(Z + 1) - 2\gamma^2}{\sqrt{(Z + 2)^2 - 4\gamma^2}}. \quad (20)$$

In Appendix A, we show that the equation $\Omega(Z) = \omega$ may have one, two, three, four, or no real roots Z_n — depending on ω and the value of the parameter γ . That is, depending on γ and ω , there can be one, two, three or four different stationary regimes of the dimer [nontrivial fixed points of the system (13)] with the given frequency. (Or there may be none.)

Namely, when $\gamma < 1$, there are four different fixed points for each $\omega > \Omega_1$, two stationary regimes with the frequency in the range $\sqrt{1 - \gamma^2} < \omega < \Omega_1$, one fixed point for each ω between $-\sqrt{1 - \gamma^2}$ and $\sqrt{1 - \gamma^2}$, and no stationary regimes if $\omega < -\sqrt{1 - \gamma^2}$. [See Fig.4(a) in the Appendix.] On the other hand, when $\gamma > 1$, the system (13) has four fixed points if $\omega > \Omega_1$, two points in the range $\Omega_3 < \omega < \Omega_1$, and no stationary regimes if $\omega < \Omega_3$. [See Fig.4(c).] Here $\Omega_1 = \Omega_1(\gamma)$ is given by equation (A4) with φ and y as in (A3), and $\Omega_3(\gamma)$ by equations (A5),(A3).

Finally, the case $\gamma = 1$ is degenerate. In this case the equation $\Omega(Z) = \omega$ has three roots when $\omega > \Omega_1$ and one root for $0 < \omega < \Omega_1$. [See Fig.4(b).] Here $\Omega_1 = \frac{1 + \sqrt{3}}{\sqrt{2}} 3^{\frac{3}{4}}$.

of the matrix (21). As ω is increased through $\sqrt{1 - \gamma^2}$ (the top boundary of the dark-grey region), another stationary solution bifurcates from the corresponding eigenvector of \mathcal{L} ,

$$\begin{pmatrix} \psi_1 \\ \psi_2 \end{pmatrix} = \begin{pmatrix} 1 \\ \sqrt{1 - \gamma^2} - i\gamma \end{pmatrix}. \quad (23)$$

As ω is raised through Ω_1 [the top boundary of the purple region in Fig.2(b)], two new stationary solutions appear “out of the clear blue sky”. It is important to note that this turning-point bifurcation is not of the saddle-centre type, as *both* newborn fixed points are centres. The centre-centre folds are not unheard of in the literature; in particular turning points separating two branches of stable solitons were reported in the context of the nonlinear Schrödinger equations with external potentials [31].

If ω is increased for the fixed $\gamma > 1$, the turning point of this type is encountered twice. First, two stable fixed points are born as ω crosses through Ω_3 [the lower bound-

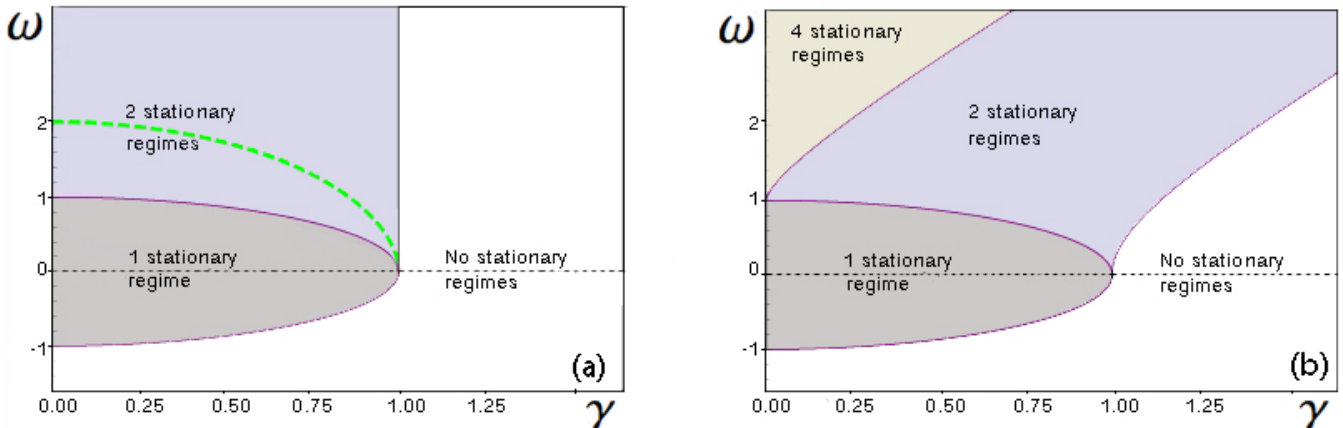


FIG. 2. The bifurcation diagram for the “standard” (linearly-coupled) \mathcal{PT} -symmetric dimer (a) and its Hamiltonian counterpart (b). The (γ, ω) plane is demarcated according to the number of co-existing roots of the equation $\Omega(Z) = \omega$. The one-root region (shaded grey) in (a) and (b) is bounded by $\omega^2 + \gamma^2 = 1$. The green dashed line in (a) is $\omega = 2\sqrt{1 - \gamma^2}$; above this line the stationary solution (27) is unstable. The two-root region (tinted purple) in (b) is bounded by $\omega = \Omega_1(\gamma)$ on the left and $\omega = \Omega_3(\gamma)$ on the right. The degeneracy line ($\gamma = 1$) featuring one or three stationary regimes is not marked in (b).

ary of the purple strip in Fig.2(b)]; second, two more centres emerge as ω passes through Ω_1 (the upper boundary of the purple region).

Another physical characteristic of the stationary regime is the total power $P = 2P_{1,2}$ carried by the pair of optical waveguides — or, alternatively, the total number of particles associated with the ground and first excited state in the BEC. Stationary regimes have $P = r/2$, with

$$r = \mathcal{R}(Z) \equiv \frac{|Z(Z+2)|}{\sqrt{(Z+2)^2 - 4\gamma^2}}. \quad (24)$$

In Appendix B, we show that depending on the value of r and parameter γ , the equation $\mathcal{R}(Z) = r$ has two, four, or no roots \tilde{Z}_n . (There is also a degenerate situation where there is one or three roots; see the next paragraph.) That is, there can be two or four stationary regimes with the same value of P . When $\gamma < 1$, there are two stationary regimes for each $r < \mathcal{R}_1(\gamma)$ and four such regimes for $r > \mathcal{R}_1(\gamma)$. [See Fig.5(a).] When $\gamma > 1$, the three-dimensional system (13) has four fixed points for any $r > \mathcal{R}_1(\gamma)$, two such points for r between $\mathcal{R}_3(\gamma)$ and $\mathcal{R}_1(\gamma)$, but no stationary regimes with $r < \mathcal{R}_3(\gamma)$. [See Fig.5(c).] These domains are demarcated in Fig.3.

As with the equation $\Omega(Z) = \omega$, the case $\gamma = 1$ is degenerate. Here the equation $\mathcal{R}(Z) = r$ has one or three roots, depending on whether r is smaller or greater than $\mathcal{R}_1(1)$ — see Fig.5(b). (Note that this degenerate situation is not delineated in Fig.3.)

VI. NONLINEAR \mathcal{PT} -SYMMETRY BREAKING

It is interesting to compare the stationary regimes of the Hamiltonian system (10) to those of the “standard”

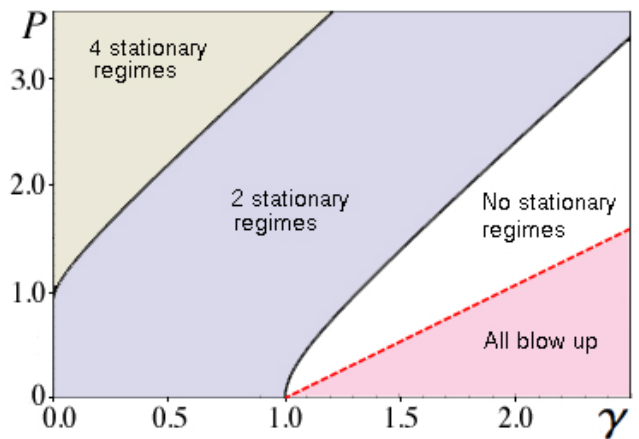


FIG. 3. The phase diagram for the Hamiltonian dimer (10). The (γ, P) plane is divided according to the numbers of co-existing stationary regimes carrying the same total power P . The boundary between the four- and two-regime phases is given by $P = \frac{1}{2}\mathcal{R}_1(\gamma)$. As this boundary is crossed from left to right, two of the four stable solutions merge and disappear. The boundary between the two-regime phase and the phase where no stationary regimes are possible, is described by $P = \frac{1}{2}\mathcal{R}_3(\gamma)$. As this boundary is crossed in the direction of larger γ , the two remaining stable stationary solutions merge and disappear. In the blank region, P either blows up or performs periodic oscillations. Dashed is the line of the \mathcal{PT} symmetry breaking transition, $\gamma = 1 + P$. In the pink region below this line, all initial conditions blow up.

\mathcal{PT} -symmetric dimer [22, 23, 27–29, 32, 33]:

$$\begin{aligned} i\dot{\psi}_1 + \psi_2 + |\psi_1|^2\psi_1 &= -i\gamma\psi_1, \\ i\dot{\psi}_2 + \psi_1 + |\psi_2|^2\psi_2 &= i\gamma\psi_2. \end{aligned} \quad (25)$$

This pair of coupled equations was used to model a variety of bimodal physical settings, where the dissipation in one mode is compensated by the energy supply in the other [3, 8, 34–38]. We note that the linearly coupled dimer (25) governs the amplitudes of the x and y oscillations in the linearly coupled oscillator system

$$\begin{aligned} \ddot{x} + 2\eta\dot{x} + x + 2\kappa y + x^3 &= 0, \\ \ddot{y} - 2\eta\dot{y} + y + 2\kappa x + y^3 &= 0. \end{aligned} \quad (26)$$

(See [39].) Equations (26) are reducible to (25) in the same way as the Hamiltonian oscillator system (2) is reducible to the Hamiltonian dimer (10).

The “standard” dimer (25) is integrable [22, 27–29]. However no Hamiltonian formulation was found for this system so far.

When γ is smaller than 1, the standard dimer exhibits two stationary regimes of the form $\psi_1 = \sqrt{P_1}e^{i\omega\tau}$, $\psi_2 = \sqrt{P_2}e^{i(\omega\tau - \theta)}$. One stationary solution is defined by

$$P_{1,2} = \omega + \sqrt{1 - \gamma^2}, \quad \theta = \pi - \arcsin \gamma;$$

it bifurcates from the eigenvector (22) as ω grows above $-\sqrt{1 - \gamma^2}$ and remains stable for all ω .

The second stationary solution has

$$P_{1,2} = \omega - \sqrt{1 - \gamma^2}, \quad \theta = \arcsin \gamma; \quad (27)$$

it bifurcates from the eigenvector (23) as ω is raised past $\sqrt{1 - \gamma^2}$ and loses stability as ω is further increased beyond $2\sqrt{1 - \gamma^2}$.

The existence and stability domains for the stationary regimes of Eq.(25) have been demarcated in Fig.2(a) — while Fig.2(b) lays out a similar bifurcation diagram for the Hamiltonian dimer (10). The most notable difference between the two panels is that stationary solutions of the linearly-coupled dimer arise only if $\gamma < 1$ [29] whereas the Hamiltonian dimer admits stable stationary regimes for arbitrarily large values of γ .

This observation suggests that the nonlinearity softens the \mathcal{PT} -symmetric phase transition in the Hamiltonian dimer. Indeed, the value $\gamma = 1$ limits the stability region of the zero solution in both models — when $\gamma > 1$, small initial conditions give rise to exponentially growing solutions. However when these small solutions have grown to become order-one (or, equivalently, when order-one initial conditions are considered), the difference between the two models becomes manifest. In the standard dimer, all non-small initial conditions blow up in the same way as the small ones whereas in its Hamiltonian counterpart, initial conditions with $|\psi_1\psi_2^* + \psi_1^*\psi_2 + 1| > \gamma$ lead to bounded trajectories.

To fully appreciate the phenomenon of nonlinear softening, it is instructive to introduce the notion of the

nonlinear analog of the \mathcal{PT} -symmetry breaking. Consider the optical system described by the nonlinear Schrödinger dimer (10) or (25), and denote $P = P_1 + P_2$ the total power carried by the pair of waveguides. We say that the system suffers the \mathcal{PT} symmetry breaking transition at the input power level P when γ is increased through the point $\gamma_c = \gamma_c(P)$ above which all initial conditions with the total power P blow up.

In the case of the standard dimer, the point of the nonlinear \mathcal{PT} -symmetry breaking is no different from the point of the linear phase transition: $\gamma_c(P) = \gamma_c(0)$ [28, 29]. In contrast, the Hamiltonian coupler carrying a finite total power P suffers its phase transition for a larger value of the gain-loss coefficient than the coupler with the infinitesimal power: $\gamma_c(P) > \gamma_c(0)$.

The exact solvability of our model allows us to find the critical value of γ for any P . Indeed, consider a ball $X^2(0) + Y^2(0) + Z^2(0) \leq r_0^2$ of initial conditions of the system (13), with the radius r_0 satisfying $(2 + r_0)^2 > 4\gamma^2$. The ball will include initial conditions lying on the horizontal planes $Z = \text{const}$ with $(2 + Z)^2 > 4\gamma^2$ and therefore leading to bounded motions. In contrast, a ball of the radius satisfying $2 + r_0 \leq 2\gamma$ cannot be cut by any horizontal planes with elliptic trajectories. Since the total power is related to the length of the vector (14) by $r = 2P$, this simple consideration gives us the critical value of the gain-loss coefficient for the given total power:

$$\gamma_c(P) = 1 + P.$$

VII. SUMMARY AND CONCLUSIONS

A. Summary of results

We have shown that a pair of coupled nonlinear oscillators, of which one oscillator has positive and the other one negative damping of equal rate, can form a Hamiltonian system, Eq.(2). Small-amplitude oscillations in this system are described by a \mathcal{PT} -symmetric nonlinear Schrödinger dimer with linear and cubic coupling, Eq.(10).

We have shown that the dimer (10) is completely integrable. Unlike the previously studied linearly-coupled model (25) (whose Hamiltonian structure has not yet been uncovered), the dimer (10) admits a Hamiltonian formulation in terms of the original variables. Unlike Eq.(25), it is exactly linearisable and solvable in elementary functions.

In systems modelled by the Hamiltonian dimer (10), the \mathcal{PT} -symmetry breaking threshold is determined by the total power: $\gamma_c = 1 + P$. The nonlinearity “softens” the \mathcal{PT} -symmetric phase transition: no matter how large is γ , there are stable periodic and quasiperiodic states (with sufficiently high power) for this gain-loss rate.

B. Concluding remarks

Two recent results are worth mentioning in the context of the present study.

The first one is due to Zezyulin and Konotop [40] who classified \mathcal{PT} -symmetric N -component oligomers with a general cubic nonlinearity. These authors prove that the nonlinearity matrix being pseudo-Hermitian with respect to the inversion \mathcal{P} is sufficient for the existence of an integral of motion bilinear in $\vec{\psi}$ and $\vec{\psi}^*$.

The dimer (10) does share this property; hence the existence of our bilinear conserved quantity $Z = 2(\psi_1\psi_2^* + \psi_1^*\psi_2)$ follows from the theory of Ref.[40]. However the second integral of motion, Eq.(12), is quartic in the fields so its existence could not be deduced from their argument.

The second relevant observation belongs to Pelinovsky, Zezyulin and Konotop [41] who have demonstrated the integrability of the following \mathcal{PT} -symmetric dimer with linear and cubic coupling:

$$\begin{aligned} i\dot{\psi}_1 + \psi_2 + (|\psi_1|^2 + |\psi_2|^2)\psi_1 &= -i\gamma\psi_1, \\ i\dot{\psi}_2 + \psi_1 + (|\psi_1|^2 + |\psi_2|^2)\psi_2 &= i\gamma\psi_2. \end{aligned} \quad (28)$$

The nonlinear dynamics exhibited by the system (28) features notable differences from that of (10).

ACKNOWLEDGMENTS

Discussions with Günter Wunner and Alexander Yanovski are gratefully acknowledged. We are also indebted to Valery Shchesnovich for instructive correspondence and Dmitry Pelinovsky for his critical reading of the manuscript. One of the authors (MG) thanks Heribert Weigert and Andy Buffler for their hospitality at the Centre for Theoretical and Mathematical Physics and Department of Physics of UCT. This project was supported by the NRF of South Africa (grants No 85751, 86991, and 87814).

Appendix A: Frequency in stationary regimes

In this appendix, we demarcate frequency ranges pertaining to the gain-loss coefficient γ smaller and greater than 1. Physically, the frequency ω represents the propagation constant of the stationary light beam and chemical potential of the boson condensate.

The frequency function (20) can be written as

$$\Omega(\mu) = \text{sign}[\mu(\mu - 2)] F(\mu), \quad (A1)$$

where

$$F(\mu) = \frac{\mu(\mu - 1) - 2\gamma^2}{\sqrt{\mu^2 - 4\gamma^2}}.$$

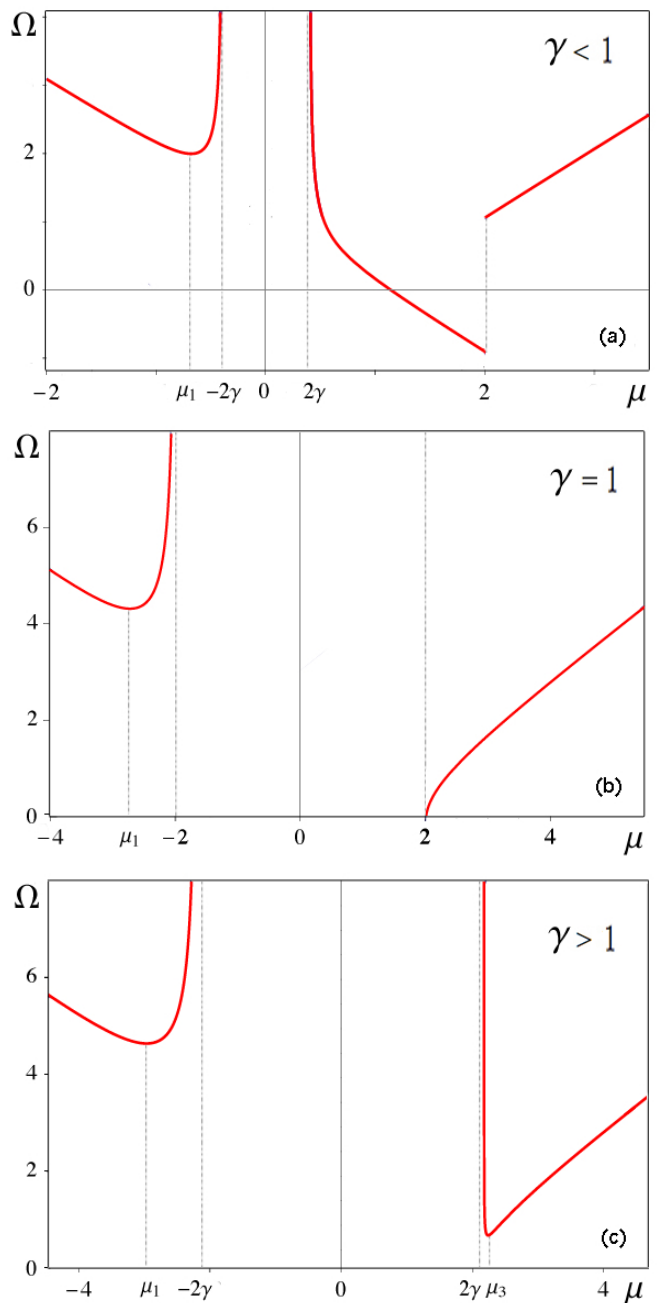


FIG. 4. Function $\Omega(\mu)$ for $\gamma < 1$ (a); $\gamma = 1$ (b); and $\gamma > 1$ (c). In (a), $\gamma = 0.2$; in (c), $\gamma = 1.1$.

Here we have introduced a parameter $\mu = Z + 2$, which changes from $-\infty$ to -2γ and from 2γ to $+\infty$. The range of frequencies admissible to the periodic solutions of the system (10) is given by the range of the function (A1).

To determine the range, we need to find the minima of $F(\mu)$. The derivative $dF/d\mu$ vanishes at the points where

$$\mu^3 - 2\gamma^2(3\mu - 2) = 0. \quad (A2)$$

Equation (A2) has one negative root μ_1 , and either 2

complex roots $\mu_2 = \mu_3^*$, or 2 positive roots $\mu_{2,3} > 0$, depending on whether $\gamma < \frac{1}{\sqrt{2}}$ or $\gamma > \frac{1}{\sqrt{2}}$.

The negative root is

$$\mu_1 = \begin{cases} -2\sqrt{2}\gamma \cosh y, & 0 < \gamma < \frac{1}{\sqrt{2}}; \\ -2\sqrt{2}\gamma \cos \varphi, & \gamma > \frac{1}{\sqrt{2}}, \end{cases}$$

where

$$y = \frac{1}{3} \operatorname{arccosh} \left(\frac{1}{\sqrt{2}\gamma} \right), \quad \varphi = \frac{1}{3} \arccos \left(\frac{1}{\sqrt{2}\gamma} \right). \quad (\text{A3})$$

As μ changes from $-\infty$ to -2γ , the function $\Omega(\mu)$ decreases from infinity, reaches a minimum equal to $\Omega_1 > 0$, where

$$\Omega_1 = \Omega(\mu_1) = \begin{cases} \frac{\gamma + \sqrt{2} \cosh y + 2\gamma \cosh(2y)}{\sqrt{\cosh(2y)}}, & 0 < \gamma < \frac{1}{\sqrt{2}}; \\ \frac{\gamma + \sqrt{2} \cos \varphi + 2\gamma \cos(2\varphi)}{\sqrt{\cos(2\varphi)}}, & \gamma > \frac{1}{\sqrt{2}}, \end{cases} \quad (\text{A4})$$

and then increases back to positive infinity. See Fig.4 (a-c).

The behaviour of $\Omega(\mu)$ in the region between 2γ and $+\infty$ depends on whether γ is smaller or greater than 1. We first note that since the factor $F(\mu)$ is growing as $\mu \rightarrow \infty$, the rightmost extremum of $F(\mu)$ has to be a minimum. However since

$$\frac{d^2 F}{d\mu^2} = 12\gamma^2 \frac{2\gamma^2 - \mu}{(\mu^2 - 4\gamma^2)^{5/2}}$$

is negative for $\mu > 2\gamma^2$, there cannot be *any* extrema to the right of $2\gamma^2$ and the continuous function $F(\mu)$ has to grow monotonically there.

When $\gamma < 1$, the value $2\gamma^2$ is to the left of 2γ . Hence the monotonicity of the factor $F(\mu)$ in the region $\mu > 2\gamma^2$ implies, in particular, that $F(\mu)$ is a monotonically growing function in the whole region $\mu > 2\gamma$. As for $\Omega(\mu)$, this discontinuous function decreases from $+\infty$ to the negative value $-\sqrt{1-\gamma^2}$ as μ grows from 2γ to 2. As μ crosses through 2, Ω jumps from $-\sqrt{1-\gamma^2}$ to $\sqrt{1-\gamma^2}$ and then grows to infinity. See Fig.4(a).

When $\gamma > 1$, the function $\Omega(\mu)$ is continuous in its entire domain of definition. As μ varies from 2γ to $+\infty$, Ω drops from infinity, reaches a minimum at some point μ_3 between 2γ and $2\gamma^2$, and grows to infinity as μ is further increased. (There can obviously be no other extrema to the right of 2γ ; had there been a maximum there, there would also have to be another minimum to the right of it, but this is impossible as the total number of positive extrema is two.) See Fig.4(c). The point of minimum is

$$\mu_3 = 2\sqrt{2}\gamma \cos \left(\frac{\pi}{3} - \varphi \right),$$

where φ is as in (A3). Denoting $\Omega_3 = \Omega(\mu_3)$, we have

$$\Omega_3 = \frac{\gamma - \sqrt{2} \cos \left(\frac{\pi}{3} - \varphi \right) + 2\gamma \cos \left(\frac{2\pi}{3} - 2\varphi \right)}{\sqrt{\cos \left(\frac{2\pi}{3} - 2\varphi \right)}}. \quad (\text{A5})$$

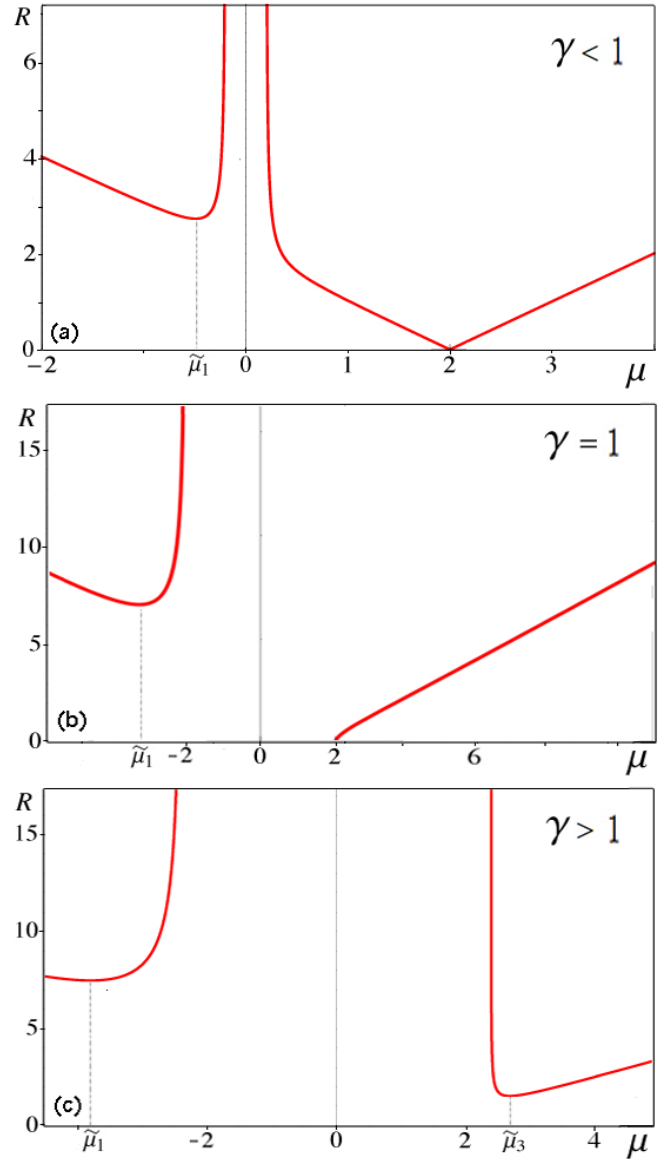


FIG. 5. Function $R(\mu)$ for $\gamma < 1$ (a), $\gamma = 1$ (b), and $\gamma > 1$ (c). In (a), $\gamma = 0.1$; in (c), $\gamma = 1.1$.

We note that if $\gamma > 1$, $F(\mu) > F(-\mu)$ holds true for any negative μ . In particular, we have $F(\mu_1) > F(-\mu_1)$, where $\mu_1 < -2\gamma$ is the point of minimum of the function $F(\mu)$ in the negative semiaxis of μ , and $-\mu_1 > 2\gamma$ is the symmetrically placed point in the positive semiaxis. This implies that the function $F(\mu)$ reaches below $F(\mu_1)$ in the region $\mu > 2\gamma$, and hence $\Omega_3 < \Omega_1$ for all $\gamma > 1$.

Appendix B: Power in stationary regimes

The aim of this appendix is to classify ranges of the admissible values of power of stationary optical beams (alternatively, numbers of particles in the condensate) described by the dimer (10).

The quantity in question is given by Eq.(24). Letting $Z + 2 = \mu$, we have

$$\mathcal{R}(Z) = R(\mu) \equiv \frac{|\mu(\mu - 2)|}{\sqrt{\mu^2 - 4\gamma^2}}.$$

The derivative $dR/d\mu$ vanishes at the points where

$$\mathcal{D}(\mu) \equiv \mu^3 - 8\gamma^2(\mu - 1) = 0.$$

This equation has one negative root $\tilde{\mu}_1 < 0$ and either two complex conjugate roots $\tilde{\mu}_2 = \tilde{\mu}_3^*$ or two positive real roots $\tilde{\mu}_{2,3} > 0$ depending on whether $\gamma < \sqrt{27/32}$ or $\gamma > \sqrt{27/32}$.

Assume, first, that $\gamma < \sqrt{27/32}$. In this case, the function $R(\mu)$ has a smooth minimum at a negative $\mu = \tilde{\mu}_1$ and a cusp at $\mu = 2$, with $R(2) = 0$ (Fig5(a)).

In the parameter range $\sqrt{27/32} < \gamma < 1$ the function $\mathcal{D}(\mu)$ has a negative minimum $\mathcal{D}(\tilde{\mu}_0) < 0$, with $\tilde{\mu}_0 = \sqrt{8/3}\gamma < 2\gamma$. Since $\mathcal{D}(2\gamma) > 0$, the two roots $\tilde{\mu}_{2,3}$ are to the left of 2γ . Therefore, in this case the derivative $dR/d\mu$ does not have any roots in the positive part of its domain of existence. The behaviour of the function $R(\mu)$ coincides with the one shown in Fig.5(a).

Finally, it remains to consider the case $\gamma > 1$. Here we have $\mathcal{D}(2), \mathcal{D}(2\gamma) < 0$ while $\mathcal{D}(0) > 0$; hence the two positive zeros of $\mathcal{D}(\mu)$ satisfy $0 < \tilde{\mu}_2 < 2$ and $\tilde{\mu}_3 > 2\gamma$. The point $\tilde{\mu}_2$ is not in the domain of $R(\mu)$ and cannot be a maximum of this function. Therefore, the function $R(\mu)$ only has two minima, at $\tilde{\mu}_1 < -2\gamma$ and $\tilde{\mu}_3 > 2\gamma$. See Fig.5(c).

Expressions for the points of local minima and the corresponding values of $R(\mu)$ are explicitly available. The left minimum is at the point

$$\tilde{\mu}_1 = \begin{cases} -\sqrt{\frac{32}{3}}\gamma \cosh \tilde{y}, & \gamma < \sqrt{\frac{27}{32}}; \\ -\sqrt{\frac{32}{3}}\gamma \cos \tilde{\varphi}, & \gamma > \sqrt{\frac{27}{32}}, \end{cases}$$

where

$$\begin{aligned} \tilde{y} &= \frac{1}{3} \operatorname{arccosh} \left(\sqrt{\frac{27}{32}} \frac{1}{\gamma} \right), & \gamma < \sqrt{\frac{27}{32}}; \\ \tilde{\varphi} &= \frac{1}{3} \arccos \left(\sqrt{\frac{27}{32}} \frac{1}{\gamma} \right), & \gamma > \sqrt{\frac{27}{32}}. \end{aligned} \quad (\text{B1})$$

The corresponding values $\mathcal{R}_1 = R(\tilde{\mu}_1)$ are

$$\begin{aligned} \mathcal{R}_1 &= 4 \left(\frac{2}{3} \right)^{\frac{3}{4}} \gamma^{\frac{1}{2}} (\cosh \tilde{y})^{\frac{3}{2}} \left[\sqrt{\frac{32}{3}} \gamma \cosh \tilde{y} + 2 \right]^{1/2}, \\ \mathcal{R}_1 &= 4 \left(\frac{2}{3} \right)^{\frac{3}{4}} \gamma^{\frac{1}{2}} (\cos \tilde{\varphi})^{\frac{3}{2}} \left[\sqrt{\frac{32}{3}} \gamma \cos \tilde{\varphi} + 2 \right]^{1/2}, \end{aligned} \quad (\text{B2})$$

for γ smaller and larger than $\sqrt{\frac{27}{32}}$, respectively.

The right local minimum (arising only if $\gamma > 1$) is at

$$\tilde{\mu}_3 = \sqrt{\frac{32}{3}} \gamma \cos \left(\frac{\pi}{3} - \tilde{\varphi} \right),$$

where $\tilde{\varphi}$ is as in (B1). The corresponding $\mathcal{R}_3 = R(\mu_3)$ is given by

$$\begin{aligned} \mathcal{R}_3 &= 4 \left(\frac{2}{3} \right)^{\frac{3}{4}} \gamma^{\frac{1}{2}} \left[\cos \left(\frac{\pi}{3} - \tilde{\varphi} \right) \right]^{\frac{3}{2}} \\ &\times \left[\sqrt{\frac{32}{3}} \gamma \cos \left(\frac{\pi}{3} - \tilde{\varphi} \right) - 2 \right]^{1/2}. \end{aligned} \quad (\text{B3})$$

Finally, when $\gamma > 1$, we have $R(\mu) > R(-\mu)$ for any negative μ in the domain of $R(\mu)$. By the argument similar to the one produced at the end of Appendix A, we conclude that $\mathcal{R}_3(\gamma) < \mathcal{R}_1(\gamma)$ for all $\gamma > 1$.

-
- [1] C M Bender and S Boettcher, Phys Rev Lett **80** 5243 (1998)
- [2] A. Guo, G. J. Salamo, D. Duchesne, R. Morandotti, M. Volatier-Ravat, V. Aimez, G. A. Siviloglou, and D. N. Christodoulides, Phys. Rev. Lett. **103**, 093902 (2009); Z. Lin, H. Ramezani, T. Eichelkraut, T. Kottos, H. Cao, and D. N. Christodoulides, Phys. Rev. Lett. **106**, 213901 (2011); L. Feng, M. Ayache, J. Huang, Y.-L. Xu, M. H. Lu, Y. F. Chen, Y. Fainman, and A. Scherer, Science **333**, 729 (2011); Y. Lumer, Y. Plotnik, M. C. Rechtsman, and M. Segev, Phys. Rev. Lett. **111** 263901 (2013); S. Longhi, Phys. Rev. A **88** 052102 (2013)
- [3] C. E. Ruter, K. G. Makris, R. El-Ganainy, D. N. Christodoulides, M. Segev, and D. Kip, Nat. Phys. **6**, 192 (2010)
- [4] S. Hu and W. Hu, J. Phys. B: At. Mol. Opt. Phys. **45** 225401 (2012); Y. He and D. Mihalache, Phys. Rev. A

- 87** 013812 (2013); Y. V. Bludov, V. V. Konotop, B. A. Malomed, Phys. Rev. A **87** 013816 (2013); G. Della Valle, S. Longhi, Phys. Rev. A **87** 022119 (2013); K. Li, D. A. Zezyulin, V. V. Konotop, P. G. Kevrekidis, Phys. Rev. A **87** 033812 (2013); X. L. Shi, F. W. Ye, B. Malomed, X. F. Chen, Opt. Lett. **38** 1064 (2013); Y. V. Bludov, R. Driben, V. V. Konotop, B. A. Malomed, Journ. Optics **15** 064010 (2013); S. Nixon, J. K. Yang, Optics Lett. **38** 1933 (2013)
- [5] H Benisty, A Degiron, A Lupu, A De Lustrac, S Chénais, S Forget, M Besbes, G Barbillon, A Bruyant, S Blaize, and G Léronnel, Optics Express **19** 18004 (2011); A. Lupu, H. Benisty, A. Degiron, Optics Express **21** 21651 (2013)
- [6] C. Hang, G. Huang, and V. Konotop, Phys. Rev. Lett. **110**, 083604 (2013); J. Sheng, M. Miri, D. N. Christodoulides, and M. Xiao, Phys. Rev. A **88**, 041803

- (2013)
- [7] S Klaiman, U Günther, and N Moiseyev, *Phys. Rev. Lett.* **101** 080402 (2008); H. Cartarius and G. Wunner, *Phys. Rev. A* **86** 013612 (2012); D Dast, D Haag, H Cartarius, J Main, and G Wunner, *J. Phys. A: Math. Theor.* **46** 375301 (2013); W D Heiss, H Cartarius, G Wunner, and J Main, *J. Phys. A: Math. Theor.* **46** 275307 (2013); D. Dast, D. Haag, H. Cartarius, G. Wunner, R. Eichler, and J. Main, *Fortschr. Phys.* **61** 124 (2013)
- [8] E.M. Graefe, H. J. Korsch, and A. E. Niederle, *Phys. Rev. Lett.* **101** 150408 (2008); E.M. Graefe, H. J. Korsch, and A. E. Niederle, *Phys. Rev. A* **82**, 013629 (2010); E.-M. Graefe, *J. Phys. A: Math. Theor.* **45** (2012) 444015
- [9] J Schindler, A Li, M C Zheng, F M Ellis, and T Kottos, *Phys Rev A* **84** 040101 (2011); J Schindler, Z Lin, J M Lee, H Ramezani, F M Ellis, T Kottos, *J Phys A: Math Theor* **45** 444029 (2012)
- [10] J. Rubinstein, P. Sternberg, and Q. Ma, *Phys. Rev. Lett.* **99**, 167003 (2007); N. Chtchelkatchev, A. Golubov, T. Baturina, and V. Vinokur, *Phys. Rev. Lett.* **109**, 150405 (2012);
- [11] S. Bittner, B. Dietz, U. Gunther, H. L. Harney, M. Miski-Oglu, A. Richter, and F. Schafer, *Phys. Rev. Lett.* **108**, 024101 (2012);
- [12] K. F. Zhao, M. Schaden, and Z. Wu, *Phys. Rev. A* **81**, 042903 (2010);
- [13] C. Zheng, L. Hao, and G. L. Long, *Phil. Trans. R. Soc. A* **371**, 20120053 (2013);
- [14] C. M. Bender, B. Berntson, D. Parker, and E. Samuel, *Am. J. Phys.* **81**, 173 (2013)
- [15] B. Peng, S. K. Ozdemir, F. Lei, F. Monifi, M. Gianfreda, G. L. Long, S. Fan, F. Nori, C. M. Bender, *L. Yang Nature Phys.* **10** 394 (2014)
- [16] N. Lazarides and G. P. Tsironis, *Phys Rev Lett* **110**, 053901 (2013); G. P. Tsironis and N. Lazarides, *Appl Phys A* **115** 449 (2014)
- [17] C. M. Bender, M. Gianfreda, Ş. K. Özdemir, B. Peng, and L. Yang, *Phys. Rev. A* **88**, 062111 (2013)
- [18] C M Bender, *Contemp. Phys.* **46** 277 (2005); *Rep. Prog. Phys.* **70** 947 (2007); A Mostafazadeh, *Int. J. Geom. Methods Mod. Phys.* **7** 1191 (2010)
- [19] A Mostafazadeh, *J. Math. Phys.* **43** 205 (2002); *J. Phys. A: Math. Gen.* **36** 7081 (2003)
- [20] C. M. Bender J.-H. Chen, D. W. Darg and K. A. Milton, *J. Phys. A: Math. Gen.* **39** 4219 (2006); C. M. Bender, D. D. Holm and D. W. Hook, *J. Phys. A: Math. Theor.* **40** F793 (2007)
- [21] S Jensen, *IEEE Journ Quant Electronics* **18** 1580 (1982); A W Snyder and Y Chen, *Opt. Lett.* **14** 517 (1989); Y Chen, A W Snyder, and D N Payne, *IEEE Journ Quant Electronics* **28** 239 (1992)
- [22] H Ramezani, T Kottos, E El-Ganainy, and D N Christodoulides, *Phys. Rev. A* **82** 043803 (2010)
- [23] A. A. Sukhorukov, Z. Xu, and Yu. S. Kivshar, *Phys. Rev. A* **82** 043818 (2010)
- [24] H. Sakaguchi and B. A. Malomed, *Phys. Rev. E* **83** 036608 (2011); N. Dror, B. A. Malomed, and J. Zeng, *Phys. Rev. E* **84** 046602 (2011)
- [25] S. Raghavan, A. Smerzi, S. Fantoni, and S. R. Shenoy, *Phys Rev A* **59** 620 (1999); D. Ananikian and T. Berge-man, *Phys Rev A* **73** 013604 (2006); I. L. Aleiner, B. L. Altshuler and Y. G. Rubo, *Phys. Rev. B* **85** 121301(R) (2012)
- [26] E. A. Ostrovskaya, Y. S. Kivshar, M. Lisak, B. Hall, F. Cattani, and D. Anderson, *Phys Rev A* **61** 031601(R) (2000); G. Theocharis, P. G. Kevrekidis, D. J. Frantzeskakis, and P. Schmelcher, *Phys. Rev. E* **74** 056608 (2006)
- [27] P G Kevrekidis, D E Pelinovsky, and D Y Tyugin, *J. Phys. A* **46** 356201 (2013)
- [28] J Pickton and H Susanto, *Phys. Rev. A* **88** 063840 (2013)
- [29] I V Barashenkov, G S Jackson, and S Flach, *Phys. Rev. A* **88** 053817 (2013)
- [30] N. V. Alexeeva, I. V. Barashenkov, K. Rayanov, and S. Flach, *Phys. Rev. A* **89** 013848 (2014)
- [31] J. Yang, *Phys. Rev. E* **85** 037602 (2012)
- [32] K. Li and P. G. Kevrekidis, *Phys. Rev. E* **83** 066608 (2011)
- [33] A. S. Rongrigues, K. Li, V. Achilleos, P. G. Kevrekidis, D. J. Frantzeskakis, C. M. Bender, *Romanian Reports in Physics* **65** 5 (2013)
- [34] R L Horne, J Cuevas, P G Kevrekidis, N Whitaker, F Kh Abdullaev, and D J Frantzeskakis, *Journ Phys A: Math Theor* **46** 485101 (2013); M. Duanmu, K. Li, R. L. Horne, P. G. Kevrekidis, N. Whitaker, *Phil. Trans. Roy. Soc. A - Math. Phys. Eng. Sci.* **371** 20120171 (2013);
- [35] S V Dmitriev, A A Sukhorukov, and Yu S Kivshar, *Opt. Lett.* **35** 2976 (2010)
- [36] K Li, P G Kevrekidis, B A Malomed, and U Günther, *J. Phys. A: Math. Theor.* **45** 444021 (2011)
- [37] R Driben and B A Malomed, *Opt. Lett.* **36** 4323 (2011); S. V. Suchkov, B. A. Malomed, S. V. Dmitriev, and Yu. S. Kivshar, *Phys. Rev. E* **84** 046609 (2011); N. V. Alexeeva, I. V. Barashenkov, A. A. Sukhorukov, and Yu. S. Kivshar, *Phys. Rev. A* **85** 063837 (2012); I. V. Barashenkov, S. V. Suchkov, A. A. Sukhorukov, S. V. Dmitriev, and Yu. S. Kivshar, *Phys. Rev. A* **86** 053809 (2012)
- [38] D. A. Zezyulin and V.V. Konotop, *Phys. Rev. Lett.* **108** 213906 (2012)
- [39] J Cuevas, P G Kevrekidis, A Saxena, A Khare, *Phys Rev A* **88** 032108 (2013)
- [40] D. A. Zezyulin and V.V. Konotop, *Journ. Phys. A: Math. Theor.* **46** (2013) 415301
- [41] D E Pelinovsky, D A Zezyulin, and V V Konotop, *J. Phys. A: Math. Theor.* **47** 085204 (2014)